Synthesis of Flavonoids using $ZnCr_2O_4$ nanoparticle catalyst

Behnam Amiri
Islamic Azad University North Tehran Branch
Roya Nazarpour
Islamic Azad University North Tehran Branch
Fouad Mohave
Islamic Azad University North Tehran Branch
Arezoo Ghaemi
Islamic Azad University, Ahvaz Branch
Haman Tavakkoli (htavakkoli59@gmail.com)
Islamic Azad University, Ahvaz Branch

Research Article

Keywords: Spinel, Flavonoid, Mesoporous, ZnCr2O4

Posted Date: April 25th, 2022

DOI: https://doi.org/10.21203/rs.3.rs-1565452/v1

Abstract

$ZnCr_2O_4$ nanoparticles with a high specific surface area has been fabricated using a hydrothermal synthetic process and was used as an effective catalyst to synthesize flavonoid derivatives. The textural and structural properties of the spinel were studied by X-ray diffraction (XRD), Field Emission scanning electron microscope (FE-SEM), nitrogen sorption techniques, and Fourier transform infrared spectroscopy (FT-IR). XRD confirmed the formation of cubic Zinc Chromite spinel with an average crystallite size of 5.04 nm. While textural analysis by N_2 sorption revealed a disordered mesoporous system with a high specific surface of 215 m^2/g for $ZnCr_2O_4$. Moreover, all desired flavonoids obtained in high yields under solvent-free conditions with the aid of the $ZnCr_2O_4$ catalyst. Structures of all flavonoid derivatives were confirmed by ^{1}H-NMR, ^{13}C-NMR, FT-IR and their melting points.

1. Introduction

Flavonoids are phenolic fused rings that can be extracted from natural resources. Due to their wide range of applications in medicine and cosmetic technology they have been the focus of countless studies so far [1]. Furthermore, these compounds are well-known for their anticancer, antioxidant, anti-inflammatory, and antitumor properties [2]. Up to now, considerable studies were carried out to take advantage of these attributes and to protect human health against diseases such as Parkinson's disease, diabetes, and Alzheimer's disease [3, 4]. More recently, in 2021, Solnier et al. [5] reported polyphenolic flavonoids which were effective against COVID. Generally, there are several methods for synthesizing flavones, chromones, and their analogs. For example, the Allan and Robinson synthesis [6] or a more common approach that involves the Baker–Venkataraman rearrangement [7] that was implemented in this paper.

Metallic nanostructures have been extensively deployed in various scientific areas based on their physico-chemical properties. However, due to their free electrons, they are less chemically stable than their oxide forms. For this reason, metal oxides nanostructure such as perovskites and spinels can be a great replacement for their metal counterparts. Spinel (AB_2O_4, A, B= Metal) mixed metal oxides are among some well-known oxide-based ceramic nanomaterials. They provide more flexible designs due to the possibility of mixing various metal oxide systems. The ability to tailor the size of particles, the morphology of nanostructure, and pore size make them a promising candidate for a broad spectrum of applications such as catalysis, sensor, energy, environment, and medicine [8-12]. Furthermore, because of the porous nature of spinel oxides, they often offer desirable attributes such as high surface area. It is well-documented that an increase in the surface area improves the catalytic activity of the catalyst due to the higher surface activity; therefore achieving this goal is in high demand for the catalysis research.

In in continuation of our previous studies in organic synthesis and mixed metal oxides [13, 14], we are reporting the synthesis of $ZnCr_2O_4$ nanoparticles with a high specific surface area. Moreover, the catalytic activity of $ZnCr_2O_4$ for the synthesis of flavonoids was investigated. Thus the aim of this study is to fabricate zinc chromate spinel and evaluate its catalytic performance.

2. Experimental

2.1 Chemicals and characterization

All chemical were obtained from Aldrich or Merck and were used without further purifications unless otherwise stated. The crystalline structure was analyzed by X-ray diffraction (D8/Advance-Bruker) using Cu Kα radiation (λ= 1.54 Å). Morphology and grain size were studied by Field-Emission Scanning electron microscope (FE-SEM) model MIRA3/XMU instrument and operated at 10 kV. Specific surface areas of the sample was determined by N_2 adsorption isotherms at 77K on a BELSORP-mini II (MicrotracBEL Corp.), the specific surface area was evaluated using the BET equation. The melting points of products were determined with an Electrothermal 9200 melting point apparatus. The FTIR was provided by Perkin Elmer BX II while the ^{1}HNMR and ^{13}CNMR spectra were provided on Bruker DRX-400 and DRX-300 Avance instruments in $CDCl_3$. The specific surface area was determined by the BET (Brunauere-Emmette-Teller) method [15], while the mesopore size distribution was calculated using BJH (Barrette-Joynere-Halenda) method [16].

2.2 Preparation of Zinc Chromite nanomaterials

In a typical synthesis, zinc nitrate ($Zn(NO_3)_2{\cdot}6H_2O$) and chromium nitrate ($Cr(NO_3)_2{\cdot}9H_2O$) were used to synthesize zinc chromite. Initially, an appropriate amount of zinc nitrate and chromium nitrate with molar compositions of the 1:2 = (Zn:Cr) were introduced into 40 mL of water to form an aqueous solution. After 15 min of vigorous stirring, NaOH was added drop-wise to adjust the pH of the solution (pH=12.0). Then the mixture was stirred for 1 hr at room temperature. Afterward, the mixture was transformed into an autoclave at 220˚C for 24 h in an electric oven without shaking or stirring. Next, the autoclave was allowed to cool to room temperature gradually. The collected precipitate was washed multiple times with ethanol and distilled water to remove any possible impurities. The final product was then heated at 80˚C and dried under vacuum for 15 h.

2.3 General procedure for the synthesis of Flavonoids

All the starting compounds 1-(2-hydroxyphenyl)-3-arylpropane-1,3-dione **4** for the synthesis of flavonoids were obtained by a two-steps procedure (scheme 1) according to the reported literature [17]. Then to synthesize flavonoids (scheme 2), 10% w/w of catalyst was mixed with 1mmol 1-(2-hydroxyphenyl)-3-arylpropane-1,3-dione and was stirred at 90˚C in solvent-free condition for 10 min. Next, the mixture was filtered and washed with CH_2Cl_2 to separate the catalyst. To afford the pure product, the solid residue was washed with petroleum ether then recrystallized from H_2O/EtOH.

2-phenyl-4H-chromen-4-one (5a, $C_{15}H_{10}O_2$). White crystals, (90%); mp 95-96 ˚C; ^{1}H NMR (250 MHz, $CDCl_3$): d 8.1-8.2 (m, 1H), 7.91-7.95 (m, 2H), 7.67-7.74 (m, 1H), 7.52-7.59 (m, 4H), 7.40-7.46 (m, 1H), 6.85 (s, 1H); ^{13}C NMR (62 MHz, $CDCl_3$): d 178.5, 163.3, 156.2, 133.8, 131.6, 129.07, 126.3, 125.7, 125.2, 118.1, 107.5.

2-(4-chlorophenyl)-4H-chromen-4-one (5b, $C_{15}H_9ClO_2$). White crystals, (95%); m.p. 190-191 ˚C; ^{1}H NMR (250 MHz, $CDCl_3$): $\delta_{H/ppm}$ 8.22-8.25 (m, 1H), 7.83-7.89 (m, 2H), 7.69-7.75 (m, 1H), 7.41-7.59 (m, 4H), 6.81 (s, 1H); ^{13}C NMR (62 MHz, $CDCl_3$): $\delta_{C/ppm}$ 178.3, 161.5, 156.1, 138.1, 133.9, 129.4, 127.5, 125.7, 125.4, 124.0, 122.9, 118.05, 107.6.

2-(4-bromophenyl)-4H-chromen-4-one (5c, $C_{15}H_9BrO_2$). White crystals, (95%); m.p. 181-182 ˚C; ^{1}H NMR (250 MHz, $CDCl_3$): $\delta_{H/ppm}$ 8.21-8.24 (m, 1H), 7.75-7.82 (m, 2H), 7.65-7.72 (m, 3H), 7.53-7.58 (m, 1H), 7.40-7.46 (m, 1H), 6.81 (s, 1H); ^{13}C NMR (62 MHz, $CDCl_3$): $\delta_{C/ppm}$ 178.2, 162.3, 156.1, 133.9, 132.3, 130.7, 127.7, 126.3, 125.7, 125.4, 123.8, 118.07, 107.6.

2-(3-chlorophenyl)-4H-chromen-4-one (5d, $C_{15}H_9ClO_2$). White crystals, (92%); m.p. 118-120 ˚C; ^{1}H NMR (250 MHz, $CDCl_3$): $\delta_{H/ppm}$ 8.20-8.24 (m, 1H), 7.91-7.93 (m, 1H), 7.68-7.8 (m, 2H), 7.43-7.59 (m, 4H), 6.8 (s, 1H); ^{13}C NMR (62 MHz, $CDCl_3$): $\delta_{C/ppm}$ 178.3, 161.8, 156.1, 135.26, 134.04, 133.5, 131.5, 130.3, 126.3, 125.7, 125.4, 124.3, 123.8, 118.1, 108.1.

2-(4-methoxyphenyl)-4H-chromen-4-one (5e, $C_{16}H_{12}O_3$). White crystals, (93%); m.p. 158-159 ˚C; ^{1}H NMR (250 MHz, $CDCl_3$): $\delta_{H/ppm}$ 8.19-8.23 (m, 1H), 7.84-7.89 (m, 2H), 7.63-7.7 (m, 1H), 7.51-7.54 (m, 1H), 7.36-7.42 (m, 1H), 6.98-7.03 (m, 2H), 6.7(s, 1H), 3.8 (s, 3H); ^{13}C NMR (62 MHz, $CDCl_3$): $\delta_{C/ppm}$ 178.3, 163.3, 162.3, 156.1, 133.5, 127.9, 125.6, 125.05, 123.98, 123.91, 117.4, 114.4, 106.1, 55.4.

2-(2,4-dichlorophenyl)-4H-chromen-4-one (5f, $C_{15}H_8Cl_2O_2$). White crystals, (97%); m.p. 129-130 ˚C; ^{1}H NMR (250 MHz, $CDCl_3$): $\delta_{H/ppm}$ 8.15-8.19 (m, 1H), 7.60-7.64 (m, 1H), 7.45-7.54 (m, 2H), 7.31-7.41 (m, 3H), 7.1 (s, 1H); ^{13}C NMR (62 MHz, $CDCl_3$): $\delta_{C/ppm}$ 177.9, 161.4, 156.5, 137.3, 134.03, 133.7, 131.3, 130.7, 130.3, 127.5, 125.7, 125.4, 123.7, 118.1, 113.1.

2-p-tolyl-4H-chromen-4-one (5g, $C_{16}H_{12}O_2$). White crystals, (93%); m.p. 112-113 ˚C; ^{1}H NMR (250 MHz, $CDCl_3$): $\delta_{H/ppm}$ 8.13-8.16 (m, 1H), 7.72-7.75 (m, 2H), 7.58-7.64 (m, 1H), 7.46-7.49 (m, 1H), 7.29-7.36 (m, 1H), 7.18-7.25 (m, 2H), 6.7 (s, 1H), 2.35 (s, 3H); ^{13}C NMR (62 MHz, $CDCl_3$): $\delta_{C/ppm}$ 178.4, 163.5, 142.1, 156.2, 133.6, 128.9, 126.2, 125.6, 125.1, 123.9, 118.04, 106.95, 21.53.

2-(2-chlorophenyl)-4H-chromen-4-one (5h, $C_{15}H_9ClO_2$). White crystals, (93%); m.p. 115-117 ˚C; ^{1}H NMR (250 MHz, $CDCl_3$): $\delta_{H/ppm}$ 8.17-8.2 (m, 1H), 7.55-7.64 (m, 3H), 7.37-7.46 (m, 3H), 7.19 (s, 1H), 6.58 (s, 1H); ^{13}C NMR (62 MHz, $CDCl_3$): $\delta_{C/ppm}$ 178.1, 162.6, 159.8, 151.3, 133.9, 132.9, 131.7, 130.8, 130.6, 127.09, 125.7, 125.3, 123.8, 118.1, 113.02.

2-(4-fluorophenyl)-4H-chromen-4-one (5i, $C_{15}H_9FO_2$). White crystals, (87%); m.p. 149-150 ˚C; ^{1}H NMR (250 MHz, $CDCl_3$): $\delta_{H/ppm}$ 8.1-8.2 (m, 1H), 7.85-7.9 (m, 2H), 7.61-7.67 (m, 1H), 7.4-7.6 (m, 1H), 7.34-7.4 (m, 1H), 7.19-7.21 (m, 2H), 6.71 (s, 1H); ^{13}C NMR (62 MHz, $CDCl_3$): $\delta_{C/ppm}$ 205.5, 174, 151.7, 148.5, 139.3, 133.8, 128.5, 125.7, 125.3, 118.01, 116.4, 116.1, 107.3.

3. Results And Discussion

3.1 Catalyst characterization

The structure and chemical species of the samples were identified by FT-IR spectroscopy Fig. 1. The FT-IR of the catalyst shows two strong signals at 500 and 613 cm^{-1} corresponding to the M–O stretching vibration, and the M–O–M bending vibration, respectively. The absence of antisymmetric NO_3^- stretching vibration and O–H stretching vibration confirms the complete transformation of nitrate salts to the desired catalyst also it indicates that the catalyst is free from any impurity.

Fig. 2 shows the X-ray diffraction patterns of $ZnCr_2O_4$. All expected peaks are observed indicating high purity of the sample. Synthesized material showed typical diffraction peaks of the pure cubic phase $ZnCr_2O_4$ spinel with $a=b=c=$ 8.33 Å. XRD pattern illustrates an intense signal corresponding to (311) plane and (220), (400), (422), (511), (440) and (533) planes (JCPDS card 22-1107).

The average crystallite size was estimated using Scherrer equation:

$$D_{hkl} = \frac{0.9\lambda}{\beta_{hkl} \cos\theta_{hkl}}$$

Where λ is radiation wavelength (nm), β (FWHW) is the difference between the full-width at half-maximum of the sample (radian) and θ is the Bragg diffraction peak angle. Crystallite size of the sample was estimated to be 5.04 nm, while lattice space $d100$($d_{100} = \lambda / 2\sin\theta$) and calculated lattice parameter ($a_o = 2d_{100}/\sqrt{3}$) were 2.51 and 2.90 nm, respectively (Table 1).

Table 1. XRD data of $ZnCr_2O_4$.

Crystal system	D_{hkl} (nm)	$d100$ (nm)	a_o (nm)
Cubic	5.04	2.51	2.90

The surface morphology of synthesized spinel was studied by FE-SEM (Fig. 3). The average grain size of the sample was estimated using the line intercept technique. SEM image illustrates that $ZnCr_2O_4$ consists of agglomerated nanoparticles with a rough surface and an average size of approximately 15 nm. Moreover, $ZnCr_2O_4$ was subjected to EDX coupled with SEM to identify the chemical composition of the synthesized solid; the EDX analysis (Fig. 4) reveals the existence of the Zn, Cr, and O elements. It also confirms the absence of any impurities.

From N_2 adsorption analysis, it is evident that the $ZnCr_2O_4$ sample presents type IV isotherm patterns, which are characteristic of mesoporous materials. According to IUPAC empirical classification [18], the hysteresis loop shown in Fig. 5 belongs to the H4 group that often denotes disordered porous materials, and their pore size and shape are not well defined. The BET surface area, total pore volume, BJH

cumulative pore volume (V_{BJH}), and mean pore diameter (D_p) were obtained from the nitrogen sorption; external surface area S_{ex} and mesopores volume V_{mes} were calculated from the *t*-plot curve. The surface area of mesoporous S_{mes} was calculated using $S_{mes} = S_{BET}-S_{ex}$ equations (Table 2). $ZnCr_2O_4$ mesoporous illustrates a high specific surface area and pore volume of 215 m^2g^{-1} and 0.19 cm^3g^{-1}, respectively, while the mean pore diameter (D_p) equals 3.6 nm, confirming the mesoporosity of the catalyst. From previous studies the reported specific surface area of the spinel $ZnCr_2O_4$ ranged from 19, 24, 30, 47, 64, 76, 96 to 117 m^2g^{-1} [19-25] while to the best of our knowledge in this paper the value of specific surface area is almost double the highest reported.

Table 2. Structural parameters of catalyst extracted from N_2 sorption.

S_{BET} (m^2g^{-1})	D_p (nm)	V_{BJH} (cm^3g^{-1})	V_{tot} (cm^3g^{-1})	S_{ex} (m^2g^{-1})	S_{mes} (m^2g^{-1})	V_{mes} (cm^3g^{-1})
215	3.6	0.17	0.19	6.46	208.54	0.18

3.2 Cyclization reaction

Initially, 1-(2-hydroxyphenyl)-3-phenylpropane-1,3-dione **4a** was selected for the model reaction to evaluate the performance of the $ZnCr_2O_4$ catalyst for the preparation of flavonoids. To optimize the reaction condition, a comparative study based on the catalyst loading, temperature, and the reaction time was performed (Table 3). Investigation in catalyst loading illustrated that the best result would be obtained when 10% (w/w) is used. Moreover, the effect of temperature on the reaction yield and time was studied. 90°C showed to be the ideal reaction temperature and applying a higher or lower temperature leads to lower yields. It is noteworthy to mention that the longer reaction time did not prove effective in the production of flavonoids. To further optimize the reaction condition, various solvent systems were tested in the model reaction (Table 4); although acetonitrile and acetone (Entry 11,12) exhibited competitive results, it was observed that the solvent-free condition is more suitable in terms of reaction time, yield, and providing a cleaner reaction condition. It can conclude that the high surface area, small size nanoparticles, and the Lewis acidic features of metals were the main driving forces behind the high catalytic activity of $ZnCr_2O_4$.

After optimization of the reaction, to explore the limitation and scope of the reaction, as can be seen from Table 5 various starting compounds **4a-4i** were used to synthesize different flavonoid derivatives **5a-5i**. As expected, it was found that the reactions of electron-withdrawing in the ortho- and para- positions yield a higher amount of flavonoids, except for (Entry 9, **4i**).

Table 3. Reaction conditions optimization.

Entry	Catalyst loading(%w/w)	Temp(°C)	Time(min)	Yield[a](%)
1	1	50	10	63
2	2	50	10	67
3	5	50	10	74
4	10	50	10	81
5	15	50	10	81
6	10	r.t	10	47
7	10	70	10	86
8	**10**	**90**	**10**	**90**
9	10	120	10	83
10	-	90	2 hr	-

[a] Isolated yield. Solvent free condition.

Table 4. Solvent effect investigation.

Entry	Solvent	Temp (°C)	Time (hr)	Yield[a] (%)
1	DMSO	Ref	24	-
2	DMF	Ref	24	-
3	Diethyl ether	Ref	24	40
4	THF	Ref	24	45
5	DCM	Ref	24	50
6	Ethanol	Ref	24	55
7	n-Hexane	Ref	24	60
8	Ethyl acetate	Ref	24	65
9	Methanol	Ref	24	70
10	Chloroform	Ref	24	70
11	Acetone	Ref	24	80
12	Acetonitrile	Ref	24	81
13	**-**	**90**	**10 min**	**90**

[a] Isolated yield. Catalyst 10% (w/w).

Based on the experimental observations and previous literatures [26, 27], the possible mechanism for the formation of flavonoids over $ZnCr_2O_4$ nanoparticles is proposed in Scheme 3. Initially, 1-(2-hydroxyphenyl)-3-arylpropane-1,3-dione **4** coordinates to the Lewis acidic site present at the catalyst surface (I). Afterward, cyclization of (II) occurs when the –OH group attacks the activated carbonyl of ketone which subsequently leads to the elimination of the water, releasing of the catalyst, and the formation of the final product **5**.

4. Conclusion

$ZnCr_2O_4$ nanoparticle with a high specific surface area has been synthesized. The structural features and properties of the synthesized spinel were reported in this paper. The porosity of the catalyst was investigated by N_2 sorption analysis. XRD detected the formation of cubic spinel with an average crystallite size of 5.04 nm. Furthermore, $ZnCr_2O_4$ was employed as a Lewis acid to synthesize flavonoid derivatives. Moreover, all desired flavonoids were obtained in high yields under solvent-free conditions. High surface area, small particle size, and Lewis acidic nature of the catalyst were the key component for the high catalytic activity of the synthesized spinel.

Declarations

Supplementary data Supplementary data associated with this article can be found in the online supplementary materials.

Author contributions All authors contributed to the study equally.

Competing interests The authors declare that they have no known competing financial interests or personal relationships that could have appeared to influence the work reported in this paper.

References

1. T. T. Cushnie, and A. J. Lamb, Antimicrobial activity of flavonoids. Int. J. Antimicrob. Agents. **26**, 343 (2005).
2. A. D. Agrawal, Pharmacological activities of flavonoids: a review. Int. J. Pharm. Sci. Nanotechnol. **4**, 1394 (2011).
3. T. Yatabe, X. Jin, K. Yamaguchi, N. Mizuno, Gold Nanoparticles Supported on a Layered Double Hydroxide as Efficient Catalysts for the One-Pot Synthesis of Flavones. Angew. Chem. Int. Ed. **54**, 13302 (2015).
4. A. K. Verma , R. Pratap, Chemistry of biologically important flavones, Tetrahedron. **68**, 8523 (2012).
5. J. Solnier, J. P. Fladerer, Flavonoids: A complementary approach to conventional therapy of COVID-19? Phytochem Rev. **20**, 773 (2021).
6. A. Banerji, N. C. Goomer, A new synthesis of flavones. Synthesis. **11**, 874 (1980).

7. K. C. Gulati, S. R. Seth, K. Venkataraman, 386. Synthetical experiments in the chromone group. Part XIII. Hydroxy-2-styrylchromones. J. Chem. Soc. **386**, 1765 (1934).
8. M. M.Thackeray, L. A. De Picciotto, A. De Kock, P. J. Johnson, V. A. Nicholas, K. T. Adendorff, Spinel electrodes for lithium batteries—a review. J. Power Sources. **21**, 1 (1987).
9. K. K. Kefeni, B. B. Mamba, T. A. Msagati, Application of spinel ferrite nanoparticles in water and wastewater treatment: a review. Sep. Purif. Technol. **188**, 399 (2017).
10. A. Šutka, K. A. Gross, Spinel ferrite oxide semiconductor gas sensors. Sens. Actuators B Chem. **222**, 95 (2016).
11. V. S. Kirankumar, S. Sumathi, A review on photodegradation of organic pollutants using spinel oxide. Mater. Today Chem. **18**, 100355 (2020).
12. M. Amiri, M. Salavati-Niasari, A. Akbari, Magnetic nanocarriers: evolution of spinel ferrites for medical applications. Adv. Colloid Interface Sci. **265**, 29 (2019).
13. A. Ghaemi, F. Mohave, A. Farhadi, M. A. Takassi, H. Tavakkoli, Hydrothermal synthesis of mesoporous cobalt ferrite by ionic liquid-assisted process; catalytic performance, morphology, and magnetic studies. J. Aust. Ceram. Soc. **57**, 1321 (2021).
14. H. Sanaeishoar, R. Nazarpour, F. Mohave, Novel one-pot pseudo four component reaction: expeditious synthesis of functionalized imidazo [1, 2-a] pyridines. RSC advances. **5**, 68571 (2015).
15. S. Brunauer, P.H. Emmett, E. Teller, J. Amer, Adsorption of gases in multimolecular layers. Chem. Soc. **60**, 309 (1938).
16. E.P. Barrett, L.G. Joyner, P.P. Halenda, The determination of pore volume and area distributions in porous substances. I. Computations from nitrogen isotherms. J. Amer. Chem. Soc. **73**, 373 (1951).
17. T. S Wheeler, Flavone. Org. Synth.**32**, 72 (2003).
18. K.S.W. Sing, D.H. Everett, RA.W. Haul, L. Moscou, R.A. Pierotti, J. Rouquerol. T. Siemieniewska, Reporting physisorption data for gas/solid systems with special reference to the determination of surface area and porosity. Pure Appl. Chem. **57**, 603 (1985).
19. M. Yang, Y. Men, S. Li, G. Chen, Enhancement of catalytic activity over TiO_2-modified Al_2O_3 and ZnO–Cr_2O_3 composite catalyst for hydrogen production via dimethyl ether steam reforming. App. Catal. A: General. **433**, 26 (2012).
20. N. Liu, Z. Yuan, C. Wang, S. Wang, C. Zhang, S. Wang, The role of CeO_2–ZrO_2 as support in the ZnO–$ZnCr_2O_4$ catalysts for autothermal reforming of methanol. Fuel Process. Technol. **89**, 574 (2008).
21. H. Tajizadegan, A. Heidary, O. Torabi, M.H. Golabgir, A. Jamshidi, Synthesis and Characterization of $ZnCr_2O_4$ Nanospinel Prepared via Homogeneous Precipitation Using Urea Hydrolysis. Int. J. Appl. Ceram. Technol. **13**, 289 (2016).
22. R. Sarkari, C. Anjaneyulu, V. Krishna, R. Kishore, M. Sudhakar, A. Venugopal, Vapor phase synthesis of methylpyrazine using aqueous glycerol and ethylenediamine over $ZnCr_2O_4$ catalyst: Elucidation of reaction mechanism. Catal. Commun. **12**, 1067 (2011).

23. A. Venugopal, R. Sarkaria, C. Anjaneyulu, V. Krishna, M.K. Kumar, N. Narender, A.H. Padmasri, Influence of acid-base sites on ZnO–$ZnCr_2O_4$ catalyst during dehydrocyclization of aqueous glycerol and ethylenediamine for the synthesis of 2-methylpyrazine: Kinetic and mechanism studies. Appl. Catal. A: General. **469**, 398 (2014).
24. W. Huang, W. Zha, D. Zhao, S. Feng, The effect of active oxygen species in nano-$ZnCr_2O_4$ spinel oxides for methane catalytic combustion. Solid State Sci.**87**, 49 (2019).
25. H. Song, D. Laudenschleger, J.J. Carey, H. Ruland, M. Nolan, M. Muhler, Spinel-structured $ZnCr_2O_4$ with excess Zn is the active ZnO/Cr_2O_3 catalyst for high-temperature methanol synthesis. ACS Catal. **7**, 7610 (2017).
26. A. S. Zambare, J. N. Sangshetti, N. D. Kokare, D. B. Shinde, Development of mild and efficient method for synthesis of substituted flavones using oxalic acid catalyst. Chin. Chem. Lett. **20**, 171 (2009).
27. K. Cheng, J. Chen, L. Jin, J. Zhou, X. Jiang, C. Yu, Rhodium (III)-catalyzed one-pot synthesis of flavonoids from salicylaldehydes and sulfoxonium ylides J. Chem. Res. **43**, 392 (2019).
28. A. P. Devi, N. Dhingra, U. Bhardwaj, R.S. Chundawat, C. K. Joshi, S. Singh, K. L.Ameta, 2-(phenyl)-4H-chromen-4-ones: Green synthesis, characterization, in vitro antifungal evaluation and molecular docking approach toward Aspergillus fumigatus. CRGSC. **5**, 100234 (2022).

Tables

Table 5 is available in the Supplemental Files section.

Figures

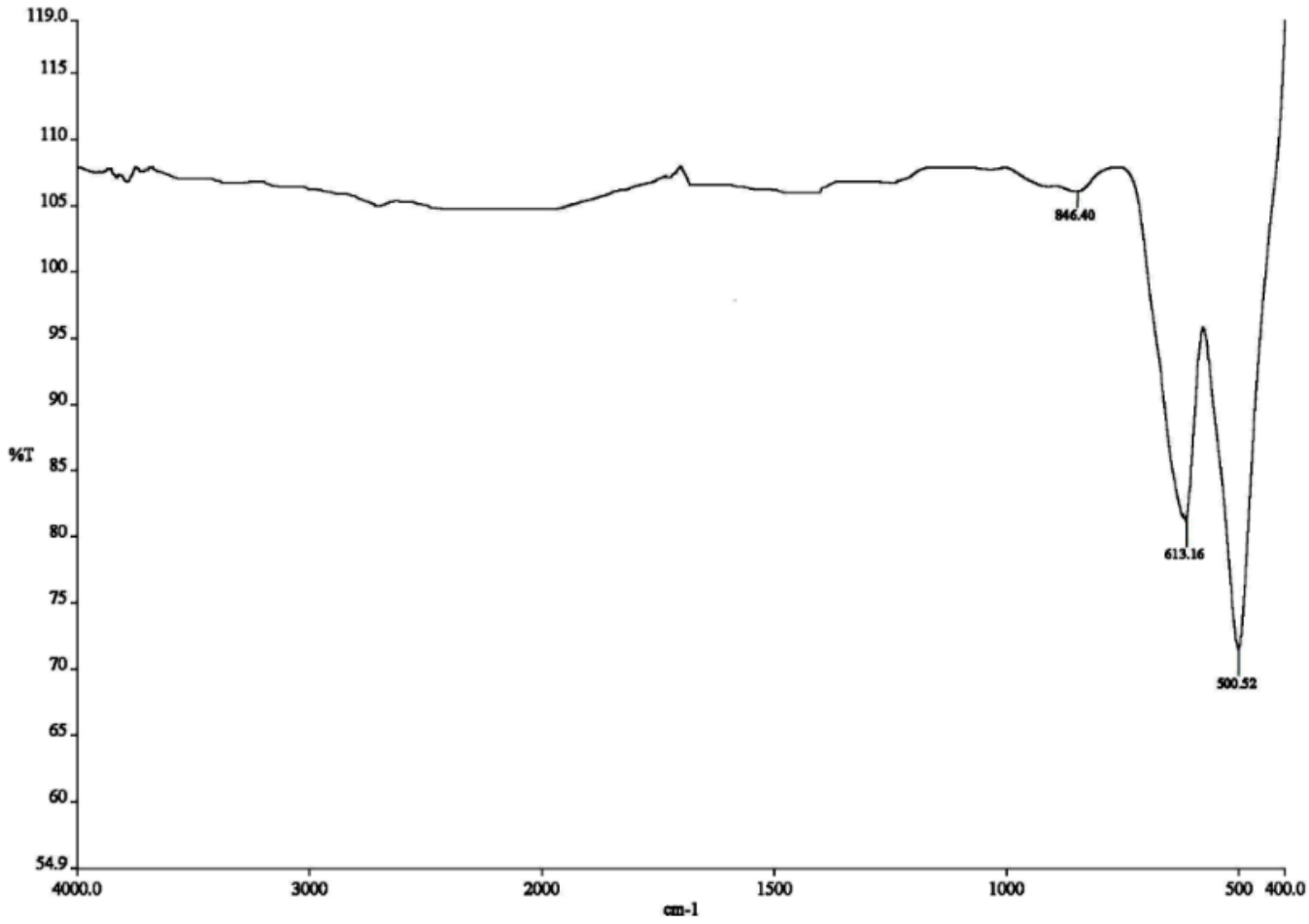

Figure 1

FT-IR spectra of $ZnCr_2O_4$.

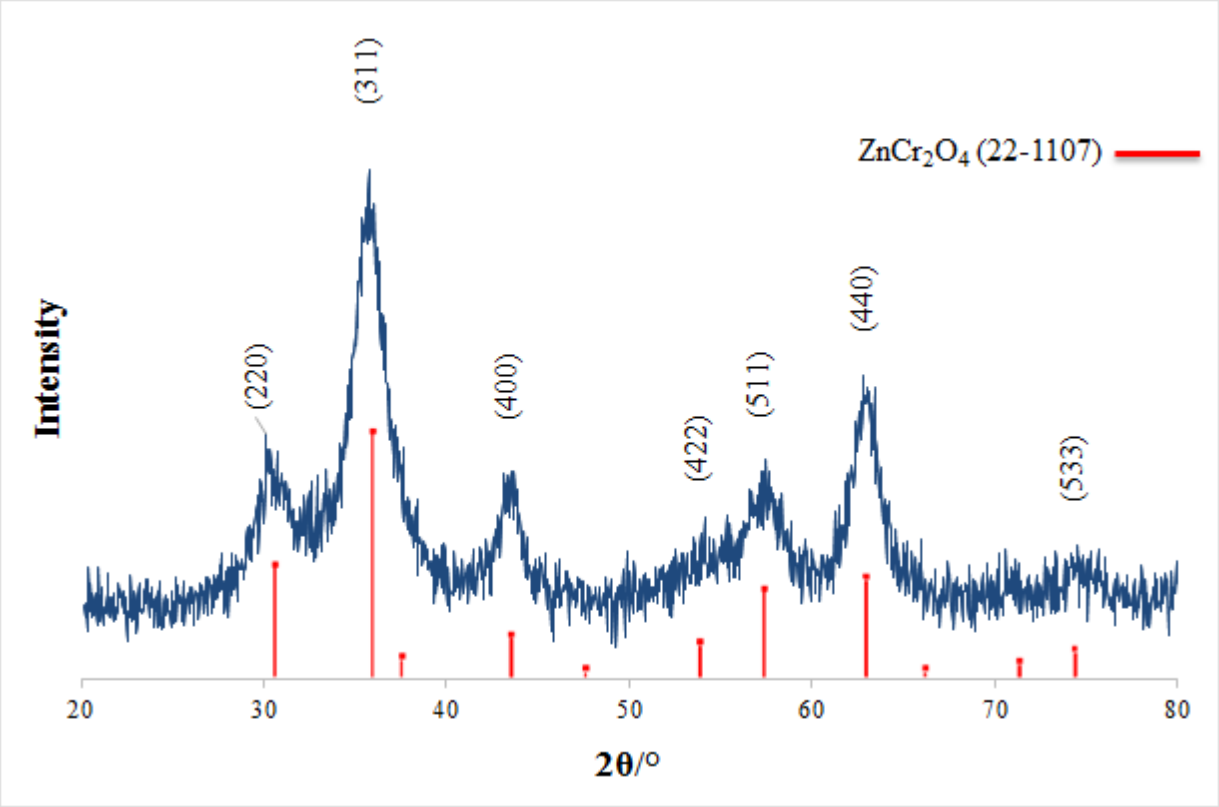

Figure 2

XRD pattern of $ZnCr_2O_4$.

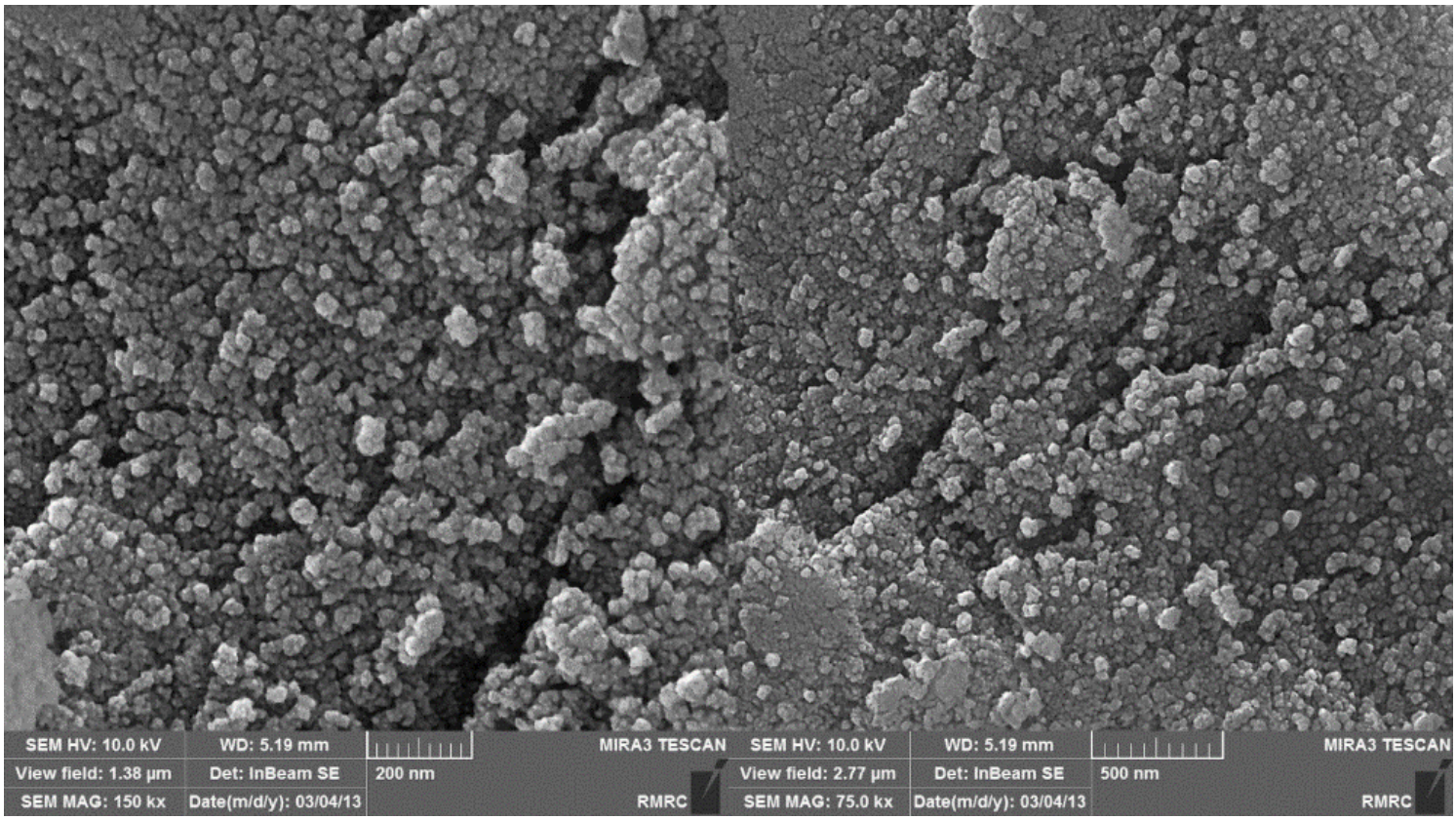

Figure 3

FE-SEM images of $ZnCr_2O_4$.

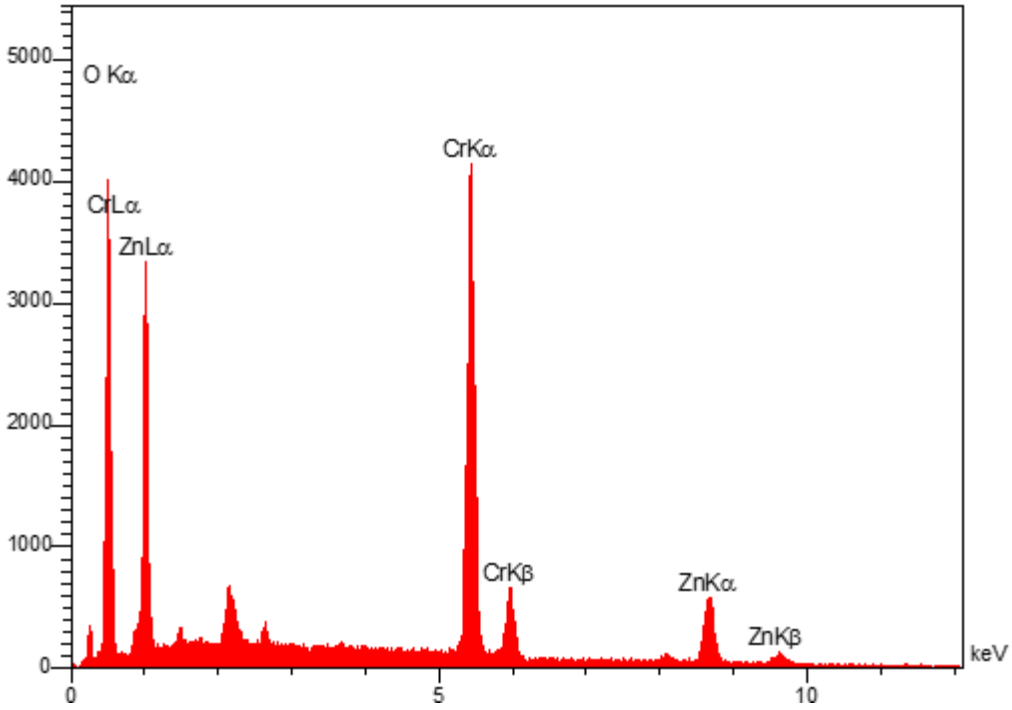

Figure 4

EDX analysis of $ZnCr_2O_4$.

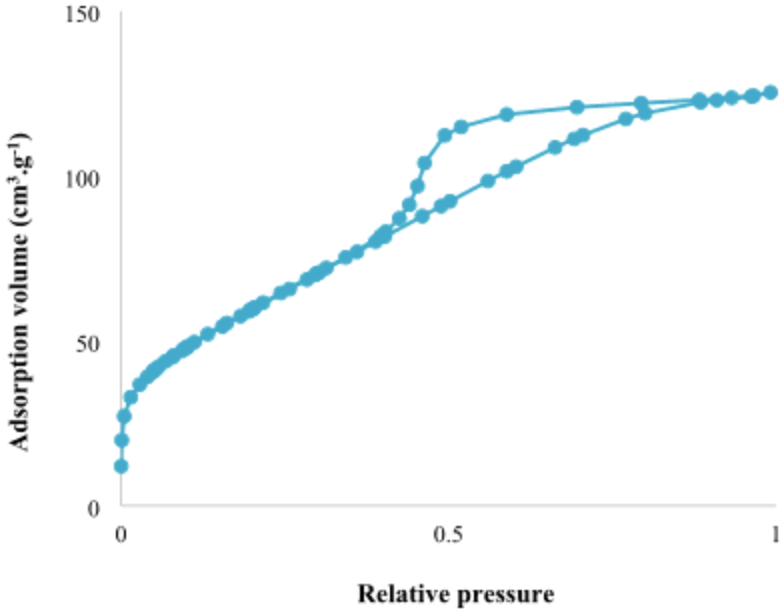

Figure 5

N_2 adsorption-desorption isotherm curves of $ZnCr_2O_4$.

Supplementary Files

This is a list of supplementary files associated with this preprint. Click to download.

- Table5.docx
- SupplementaryData.docx